

Nonequilibrium dynamics in the antiferromagnetic Hubbard model

Matteo Sandri and Michele Fabrizio

International School for Advanced Studies (SISSA), and CRS Democritos, CNR-INFM, Via Bonomea 265, I-34136 Trieste, Italy

(Received 21 June 2013; revised manuscript received 2 September 2013; published 8 October 2013)

We investigate by means of the time-dependent Gutzwiller variational approach the out-of-equilibrium dynamics of an antiferromagnetic state evolved with the Hubbard model Hamiltonian after a sudden change of the repulsion strength U . We find that magnetic order survives more than what is expected on the basis of thermalization arguments, in agreement with recent dynamical mean field theory calculations. In addition, we find evidence of a dynamical transition for quenches to large values of U between a coherent antiferromagnet characterized by a finite quasiparticle residue to an incoherent one with vanishing residue, which finally turns into a paramagnet for even larger U .

DOI: [10.1103/PhysRevB.88.165113](https://doi.org/10.1103/PhysRevB.88.165113)

PACS number(s): 71.10.Fd, 71.30.+h, 64.60.Ht

I. INTRODUCTION

In the last years the out-of-equilibrium physics in correlated systems has attracted considerable interest, mainly driven by impressive experimental progresses. On one hand, trapped cold atoms, known to effectively realize simple model Hamiltonians, have been successfully exploited to investigate quench dynamics or field-driven nonequilibrium phenomena in quasi-isolated quantum many-body systems.¹ On the other hand, time-resolved femtosecond spectroscopies have made it possible to perturb solid-state systems and access the dynamics of the electronic degrees of freedom before they thermalize with the environment and even before they equilibrate with the lattice.² Overall, these experiments allow us to study how strong correlation affects the out-of-equilibrium physics and possibly identify “novel phases” that can not be reached by conventional thermal pathways. To this end, a fundamental issue to address is the real-time dynamics across a phase transition in which symmetry is broken or restored. The ultrafast melting and creation of long-range order in transition-metal compounds has already been investigated in many experiments.^{3–5} On the theoretical side, however, while an equilibrium phase transition is a well-established concept, there is yet no clear extension to the out-of-equilibrium case.⁶ The common viewpoint is that the initial excess energy ΔE turns into heat, hence the system evolves into a thermal state at a higher effective temperature T_* , which is higher the bigger ΔE is. Should T_* exceed the critical temperature for a order-to-disorder phase transition, the system would dynamically disorder although it was initially ordered.

Recently, the dynamics of a symmetry-breaking state has been addressed by means of time-dependent dynamical mean field theory (DMFT) in the single-band repulsive Hubbard model on a Bethe lattice.^{7,8} Such a model, which may be considered as the simplest idealization of strongly correlated electrons, displays at equilibrium a Néel transition from a low-temperature antiferromagnet (AFM) to a high-temperature paramagnet (PM). As mentioned, upon the sudden changing of the interaction strength $U_i \rightarrow U_f$, one could dynamically move around the phase diagram and eventually cross the Néel transition. References 7 and 8 showed that both for $U_f < U_i$ and $U_f > U_i$, long-lived nonthermal ordered states exist even though their expected T_* is above the Néel temperature T_N . Moreover, it was found that for $U_f < U_i$, the melting of the

AFM order is related to the existence of a nonthermal critical point with an associated vanishing amplitude mode. Both these features are a consequence of pure nonequilibrium effects.

Here, we address the same model dynamics by means of the time-dependent Gutzwiller variational approach introduced in Ref. 9. This method, although being less accurate than DMFT, is computationally far less expensive and has already proved its reliability in reproducing the main results of DMFT in the out-of-equilibrium dynamics of paramagnetic states.^{9–11} We find that also in the broken-symmetry dynamics, the time-dependent Gutzwiller technique correctly reproduces both the presence of a critical point at which magnetism disappears as well as the existence of nonthermal ordered states. Moreover, we find evidence of an additional critical point at $U_f > U_i$ between two antiferromagnetic states that we interpret as the magnetic analog of a dynamical Mott transition.

The paper is organized as follows. In Sec. II, we briefly present how the method works in the specific case of an antiferromagnet. In Sec. III, we move to discuss the results of a quench from an initial magnetic state, ground state of the Hamiltonian at repulsion U_i , evolved with the Hamiltonian at a different value U_f , both for $U_f < U_i$ (Sec. III A) and $U_f > U_i$ (Sec. III B). Finally, Sec. IV is devoted to conclusions.

II. TIME-DEPENDENT GUTZWILLER

In this section, we briefly show how the time-dependent Gutzwiller technique introduced in Ref. 9 has to be modified to treat the AFM dynamics within the single-band Hubbard model at half-filling, with Hamiltonian

$$\mathcal{H} = - \sum_{(\mathbf{R}, \mathbf{R}'), \sigma} (c_{\mathbf{R}\sigma}^\dagger c_{\mathbf{R}'\sigma} + \text{H.c.}) + \frac{U(t)}{2} \sum_{\mathbf{R}} (n_{\mathbf{R}} - 1)^2, \quad (1)$$

where $c_{\mathbf{R}\sigma}$ annihilates a spin- σ electron at site \mathbf{R} , $U(t)$ is the (time-dependent) interaction strength, and $n_{\mathbf{R}} = \sum_{\sigma} c_{\mathbf{R}\sigma}^\dagger c_{\mathbf{R}\sigma}$. The hopping parameter is set equal to one and is our unit of energy. We follow the same notations as Ref. 12, to which the reader is referred for a more detailed derivation. The main idea of the time-dependent Gutzwiller technique is to approximate the evolving wave function $|\Psi(t)\rangle$ in terms of a variational wave function whose dynamics is set by requiring

the stationarity of the real-time action

$$\mathcal{L}(t) = \int_0^t d\tau \langle \Psi(\tau) | i\partial_\tau - \mathcal{H}(\tau) | \Psi(\tau) \rangle. \quad (2)$$

In the same spirit of the ground-state Gutzwiller method, one introduces the following ansatz for the evolving wave function:⁹

$$|\Psi(t)\rangle = \prod_{\mathbf{R}} \mathcal{P}_{\mathbf{R}}(t) |\psi(t)\rangle, \quad (3)$$

where $|\psi(t)\rangle$ is a generic time-dependent variational Slater determinant, and $\mathcal{P}_{\mathbf{R}}(t)$ a time-dependent variational local operator.

Upon introducing a basis for the local Fock space

$$|\mathbf{R}, \{n\}\rangle = \prod_{\alpha=\uparrow,\downarrow} (c_{\mathbf{R}\alpha}^\dagger)^{n_\alpha}, \quad (4)$$

one can parametrize the Gutzwiller projector in terms of a set of time-dependent variational parameters $\Phi_{\mathbf{R}\{n\}}(t)$:

$$\mathcal{P}_{\mathbf{R}}(t) = \sum_{\{n\}} \frac{\Phi_{\mathbf{R}\{n\}}(t)}{\sqrt{P_{\mathbf{R}\{n\}}^{(0)}(t)}} |\mathbf{R}, \{n\}\rangle \langle \mathbf{R}, \{n\}|, \quad (5)$$

where

$$P_{\mathbf{R}\{n\}}^{(0)}(t) = \langle \psi(t) | \mathbf{R}, \{n\} \rangle \langle \mathbf{R}, \{n\} | \psi(t) \rangle. \quad (6)$$

In Ref. 12 it was shown that the stationarity of (2) amounts to solve a set of coupled differential equations that determine the evolution of the uncorrelated wave function $|\psi(t)\rangle$ and the variational parameters $\Phi_{\mathbf{R}\{n\}}(t)$:

$$i\partial_t |\psi(t)\rangle = \mathcal{H}_*[\hat{\Phi}(t)] |\psi(t)\rangle, \quad (7)$$

$$i\partial_t \hat{\Phi}_{\mathbf{R}}(t) = \hat{U}(t) \hat{\Phi}_{\mathbf{R}}(t) + \langle \psi(t) | \frac{\partial \mathcal{H}_*[\hat{\Phi}(t)]}{\partial \hat{\Phi}_{\mathbf{R}}^\dagger(t)} | \psi(t) \rangle. \quad (8)$$

With the notation $\hat{O}_{\mathbf{R}}$ we indicate the matrix representation of the operator $O_{\mathbf{R}}$ on the Fock basis (4). If we assume the magnetization directed along z , then we can choose $\hat{\Phi}_{\mathbf{R}}$ to be a diagonal matrix with diagonal elements $\Phi_{\mathbf{R}\{0\}}$, for empty site, $\Phi_{\mathbf{R}\{\uparrow\}}$ and $\Phi_{\mathbf{R}\{\downarrow\}}$, for singly occupied site with a spin-up or -down electron, respectively, and finally $\Phi_{\mathbf{R}\{\uparrow\downarrow\}}$ for a doubly occupied site.

The Slater determinant evolves according to a ‘‘renormalized’’ one-body Hamiltonian

$$\mathcal{H}_*[\hat{\Phi}(t)] = - \sum_{(\mathbf{R}, \mathbf{R}'), \sigma} (R_{\mathbf{R}\sigma}^*(t) c_{\mathbf{R}\sigma}^\dagger R_{\mathbf{R}'\sigma}(t) c_{\mathbf{R}'\sigma} + \text{H.c.}), \quad (9)$$

which is self-consistently coupled to the evolution of the matrix $\hat{\Phi}_{\mathbf{R}}(t)$ through the renormalization factors

$$R_{\mathbf{R}\sigma}(t) = \frac{1}{\sqrt{n_{\mathbf{R}\sigma}(t)[1 - n_{\mathbf{R}\sigma}(t)]}} \text{Tr}[\hat{\Phi}_{\mathbf{R}}^\dagger(t) \hat{c}_{\mathbf{R}\sigma} \hat{\Phi}_{\mathbf{R}\sigma}(t) \hat{c}_{\mathbf{R}\sigma}^\dagger]. \quad (10)$$

In the presence of Néel AFM order, we can separate the bipartite lattice into two sublattices A and B such that Eq. (9) becomes

$$\mathcal{H}_*(t) = - \sum_{(\mathbf{R}_a, \mathbf{R}_{\bar{a}}), \sigma} (R_{\mathbf{R}_a\sigma}^*(t) R_{\mathbf{R}_{\bar{a}}-\sigma}(t) c_{\mathbf{R}_a\sigma}^\dagger c_{\mathbf{R}_{\bar{a}}\sigma} + \text{H.c.}), \quad (11)$$

where if $a = A$ then $\bar{a} = B$ and vice versa, and we make use of

$$R_{\mathbf{R}_a\sigma} = R_{\mathbf{R}_{\bar{a}}-\sigma}, \text{ with } a \in \{A, B\}. \quad (12)$$

It is more convenient to work in Fourier space where Eq. (11) reads as

$$\mathcal{H}_*(t) = \sum_{\mathbf{k}\sigma} \varepsilon(\mathbf{k}) [\text{Re}(R_{\mathbf{R}_a\sigma}^*(t) R_{\mathbf{R}_{\bar{a}}-\sigma}(t)) c_{\mathbf{k}\sigma}^\dagger c_{\mathbf{k}\sigma} - i \text{Im}(R_{\mathbf{R}_a\sigma}^*(t) R_{\mathbf{R}_{\bar{a}}-\sigma}(t)) c_{\mathbf{k}\sigma}^\dagger c_{\mathbf{k}+\mathbf{Q}\sigma}] \quad (13)$$

with $\varepsilon(\mathbf{k}) = \frac{1}{N} \sum_{(\mathbf{R}_a, \mathbf{R}_{\bar{a}})} e^{i\mathbf{k}\cdot(\mathbf{R}_a - \mathbf{R}_{\bar{a}})}$ where N is the number of sites, and the vector \mathbf{Q} such that

$$e^{i\mathbf{Q}\cdot\mathbf{R}_a} = \begin{cases} 1 & \text{if } a \in A, \\ -1 & \text{if } a \in B. \end{cases} \quad (14)$$

The time evolution of the uncorrelated $|\psi(t)\rangle$ can then be recasted into that of $\Delta_{\mathbf{k}\mathbf{k}'}^\sigma(t) := \langle \psi(t) | c_{\mathbf{k}\sigma}^\dagger c_{\mathbf{k}'\sigma} | \psi(t) \rangle$ whose equations of motion are

$$\begin{aligned} i\partial_t \Delta_{\mathbf{k}\mathbf{k}}^\sigma &= -i\varepsilon(\mathbf{k}) \text{Im}[Z^\sigma(t)] (\Delta_{\mathbf{k}\mathbf{k}+\mathbf{Q}}^\sigma + \Delta_{\mathbf{k}+\mathbf{Q}\mathbf{k}}^\sigma), \\ i\partial_t \Delta_{\mathbf{k}\mathbf{k}+\mathbf{Q}}^\sigma &= -2\varepsilon(\mathbf{k}) \text{Re}[Z^\sigma(t)] \Delta_{\mathbf{k}\mathbf{k}+\mathbf{Q}}^\sigma \\ &\quad + i\varepsilon(\mathbf{k}) \text{Im}[Z^\sigma(t)] (\Delta_{\mathbf{k}\mathbf{k}}^\sigma - \Delta_{\mathbf{k}+\mathbf{Q}\mathbf{k}+\mathbf{Q}}^\sigma). \end{aligned} \quad (15)$$

To simplify notations, we introduced the quantity $Z^\sigma(t) = R_{\mathbf{R}_a\sigma}^*(t) R_{\mathbf{R}_{\bar{a}}-\sigma}(t)$. By construction, it follows that

$$n_{A(B)\sigma}(t) = \frac{1}{N} \sum_{\mathbf{k}} \Delta_{\mathbf{k}\mathbf{k}}^\sigma(t) \pm \Delta_{\mathbf{k}\mathbf{k}+\mathbf{Q}}^\sigma(t). \quad (16)$$

The evolution of the uncorrelated wave function is self-consistently coupled to Eq. (8) that, because of (12), can be evaluated for a single sublattice and reads as

$$\begin{aligned} i\frac{\partial \hat{\Phi}_A}{\partial t} &= \hat{U} \hat{\Phi}_A(t) \\ &\quad + \frac{1}{N} \sum_{\mathbf{k}, \sigma} \varepsilon(\mathbf{k}) \left[R_{A-\sigma} (\Delta_{\mathbf{k}\mathbf{k}}^\sigma(t) - \Delta_{\mathbf{k}\mathbf{k}+\mathbf{Q}}^\sigma(t)) \frac{\partial R_{A\sigma}^*}{\partial \hat{\Phi}_A^\dagger} \right. \\ &\quad \left. + R_{A-\sigma}^* (\Delta_{\mathbf{k}\mathbf{k}}^\sigma(t) + \Delta_{\mathbf{k}\mathbf{k}+\mathbf{Q}}^\sigma(t)) \frac{\partial R_{A\sigma}}{\partial \hat{\Phi}_A^\dagger} \right]. \end{aligned} \quad (17)$$

In conclusion, Eqs. (15)–(17) together with Eqs. (10) and (16) define a set of coupled nonlinear differential equations which must be solved numerically.

In spite of the nonlinearity, the dynamics is still oversimplified and we do not expect to reach thermalization in the long-time limit, mainly because the evolution of the Slater determinant still admits an infinite number of integrals of motion. In fact, the dynamics of $|\psi(t)\rangle$ does not mix different $(\mathbf{k}, \mathbf{k} + \mathbf{Q})$ subspaces. Within each subspace, the set of equations (15) can be mapped onto the dynamics of a pseudospin- $\frac{1}{2}$ Hamiltonian. Indeed, upon defining

$$\begin{aligned} \Delta_{\mathbf{k}\mathbf{k}}^\sigma - \Delta_{\mathbf{k}+\mathbf{Q}\mathbf{k}+\mathbf{Q}}^\sigma &\equiv \langle \sigma_1 \rangle, \\ \Delta_{\mathbf{k}\mathbf{k}+\mathbf{Q}}^\sigma + \Delta_{\mathbf{k}+\mathbf{Q}\mathbf{k}}^\sigma &\equiv \langle \sigma_2 \rangle, \\ \Delta_{\mathbf{k}\mathbf{k}+\mathbf{Q}}^\sigma - \Delta_{\mathbf{k}+\mathbf{Q}\mathbf{k}}^\sigma &\equiv -i \langle \sigma_3 \rangle \end{aligned}$$

[where in this case \mathbf{k} is restricted to the magnetic Brillouin zone (MBZ)], the set of equations (15) is equivalent to solving the dynamics of the pseudospin Hamiltonian

$$\mathcal{H}_{\mathbf{k}\sigma}^S(t) = \varepsilon(\mathbf{k}) \text{Im}[Z_\sigma(t)] \sigma_3 - \varepsilon(\mathbf{k}) \text{Re}[Z_\sigma(t)] \sigma_1, \quad (18)$$

where $\sigma_{1,2,3}$ are Pauli matrices. Indeed, as we mentioned, the length of the pseudospin is a conserved quantity in each subspace.

It is generally believed that the average values of local operators along the unitary evolution of a wave function $|\Psi\rangle$, generically consisting of a superposition of a macroscopic number of eigenstates, will approach at long times the thermal averages on a Boltzmann-Gibbs distribution at an effective temperature T_* for which the internal energy coincides with the energy of the wave function $|\Psi\rangle$, conserved during the unitary evolution, i.e.,

$$\frac{\text{Tr}(e^{-\mathcal{H}/T_*} \mathcal{H})}{\text{Tr}(e^{-\mathcal{H}/T_*})} = \langle \Psi | \mathcal{H} | \Psi \rangle.$$

Therefore, it is worth comparing the results of the time-dependent Gutzwiller technique with equilibrium results at finite temperature obtained by a similar technique. For that purpose, we shall make use of an extension to finite temperature of the Gutzwiller variational approach recently proposed.¹³ In brief, the thermal values are computed minimizing the following variational estimate of the free energy:

$$F \leq \min_{\{\rho_*, \hat{\Phi}\}} \left\{ \sum_{(\mathbf{R}, \mathbf{R}')} \text{Tr}[\rho_* (-R_{\mathbf{R}\sigma} R_{\mathbf{R}'\sigma}^\dagger c_{\mathbf{R}\sigma} c_{\mathbf{R}'\sigma} + \text{H.c.})] + \sum_{\mathbf{R}} \text{Tr}(\hat{\Phi}_{\mathbf{R}}^\dagger \hat{U} \hat{\Phi}_{\mathbf{R}}) - T \text{Max}(S_{\text{var}}(\rho_*, \hat{\Phi}^\dagger \hat{\Phi}), 0) \right\}, \quad (19)$$

where $\rho_* = e^{-\beta \mathcal{H}_*} / (\text{Tr} e^{-\beta \mathcal{H}_*})$ is the Boltzmann distribution corresponding to the variational Hamiltonian \mathcal{H}_* , and the variational estimate of the entropy reads as

$$S_{\text{var}}(\rho_*, \hat{\Phi}^\dagger \hat{\Phi}) = -\text{Tr}(\rho_* \ln \rho_*) - \sum_{\mathbf{R}, \{n\}} |\Phi_{\mathbf{R}n}|^2 \ln \left(\frac{|\Phi_{\mathbf{R}n}|^2}{P_{\mathbf{R}n}^{(0)}} \right). \quad (20)$$

We conclude this section remarking that all the above treatment is strictly variational only in the limit of infinite coordination number, where the exact averages on the Gutzwiller variational wave function (or the thermal averages on the variational canonical distribution) coincide with those we have computed.¹² However, the approach remains essentially a mean field one, hence, although improves the time-dependent Hartree-Fock approximation simply because of the larger number of variational parameters, it misses dissipative processes that in reality bring the system to a stationary state. In spite of that, the Gutzwiller approach seems to reproduce quite satisfactorily the main results obtained by exact DMFT calculations, whenever a comparison is possible and even when time-dependent Hartree-Fock fails completely, like in the case of quantum quenches within the paramagnetic sector.⁹

In finite coordination lattices, the approach is not anymore variational. Nevertheless, it is common to keep using the same expressions also in these more physical cases, which goes under the name of *Gutzwiller approximation*. Even though to our knowledge there are so far no exact out-of-equilibrium results to compare with in finite coordination lattices, recent high-order perturbative calculations in one and two dimensions^{14,15} bring results quite similar to those obtained in Ref. 9 through the Gutzwiller approach. At equilibrium, instead, the Gutzwiller approximation seems to reproduce well exact variational Monte Carlo calculations

on the Gutzwiller wave functions,¹⁶ and, when applied in combination with *ab initio* density functional theory methods, also physical properties of real materials.¹⁷

III. INTERACTION QUENCH

In this section, we apply the time-dependent Gutzwiller approach to study the dynamics of (1) after a sudden quench of the interaction strength $U(t) = U_i + (U_f - U_i)\theta(t)$, where $\theta(t)$ is the Heaviside function. Although an instantaneous quench is distant from the real practice in experiments, it is a well-controlled theoretical excitation protocol and suffices well the scope of this work. We assume nearest-neighbor hopping on an infinitely branched Bethe lattice, i.e., a semicircular density of states $D(\varepsilon) = \sqrt{4 - \varepsilon^2} / (2\pi)$, in which case the Gutzwiller approximation becomes exact. We remark that the momentum representation we previously adopted is not appropriate for a Bethe lattice, but can be easily extended in this case.

In Fig. 1, we plot the finite-temperature phase diagram for the model as found by means of the finite-temperature extension of the Gutzwiller technique.¹³ We see that the low-temperature AFM-ordered phase compares qualitatively well with the DMFT results.⁸ In particular, the Gutzwiller wave function is able, unlike straight Hartree-Fock, to describe a finite-temperature Mott-insulating phase devoid of magnetism.

A. $U_f < U_i$ quench

We start by analyzing the dynamics for quenches at $U_f < U_i$. We plot in Fig. 2 the time evolution of the AFM order parameter $m = n_\uparrow - n_\downarrow$ for an interaction quench starting from the optimized variational ground state at $U_i = 4.0$. We immediately recognize a pattern which is very similar to that obtained within DMFT and Hartree-Fock dynamics.⁸

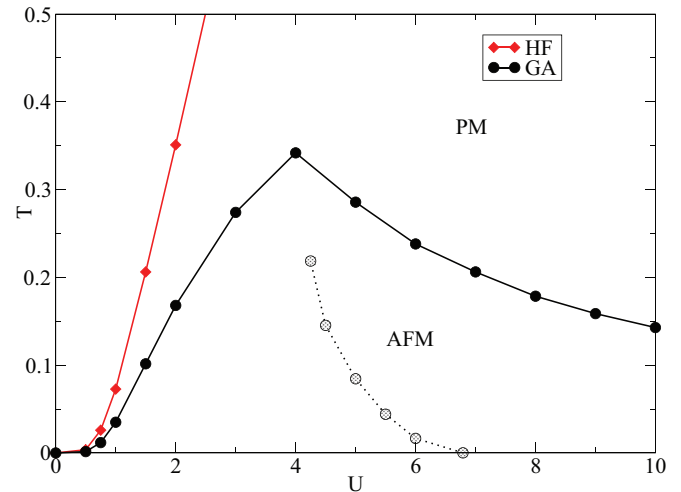


FIG. 1. (Color online) Finite-temperature phase diagram for the single-band Hubbard model as obtained by means of the finite-temperature Gutzwiller approach. The solid black line separates the AFM solution from the PM phase. The dotted line indicates the metal-insulator transition (MIT) transition when only paramagnetic states are considered. The red line is the Néel temperature within the Hartree-Fock approximation.

The order parameter $m(t)$ quickly decreases in time after the quench and starts oscillating; as U_f decreases below the critical value of $U_c^{U_f < U_i} \approx 1.7$, the order parameter vanishes.

On the same figure we also plot the thermal values m_{th} calculated from the finite-temperature Gutzwiller approach¹³ at an effective temperature T_* such that the equilibrium internal energy is equal to the average energy on the variational wave function, which is conserved by the unitary evolution. We note that $m(t)$ oscillates around a value which is more and more distant from the thermal one and stays finite even when T_* exceeds the Néel temperature, suggesting that the dynamics stays trapped in a nonthermal ordered state in accordance with DMFT result.⁸ From Fig. 2, two well-separated frequencies are distinguishable in the dynamics, which we extract by a discrete Fourier transform and plot in Fig. 5. A high frequency ω_1 sets the fast oscillation and decreases with U_f , although staying finite. A lower frequency ω_2 can instead be associated to the presence of magnetic order and vanishes at the critical point as $\propto |U_f - U_c^{U_f < U_i}|$; the existence of a linearly vanishing mode was found also in Ref. 8.

This two-frequency dynamics reveals the mechanism beyond the disappearance of the AFM order at $U_c^{U_f < U_i}$. This is more clearly shown in Fig. 3 where we plot the values of the real and imaginary parts of the renormalization factors. We observe that approaching $U_c^{U_f < U_i}$, the renormalization factors show main oscillations with frequency ω_2 , on top of which there are much narrower oscillations controlled by ω_1 . In proximity of $U_c^{U_f < U_i}$, $\omega_1 \gg \omega_2 \rightarrow 0$, so that, within each $(\mathbf{k}, \mathbf{k} + \mathbf{Q})$ subspace, the magnetic field in the pseudospin Hamiltonian (18) can be effectively taken constant in time. Hence, the dynamics of (18) is equivalent to that of a spin in the presence of a \mathbf{k} -dependent constant magnetic field. The total staggered magnetization then vanishes due to the dephasing that occurs summing on the entire Brillouin zone, hence the nature of the critical point is essentially that found within the Hartree-Fock approximation by Ref. 8.

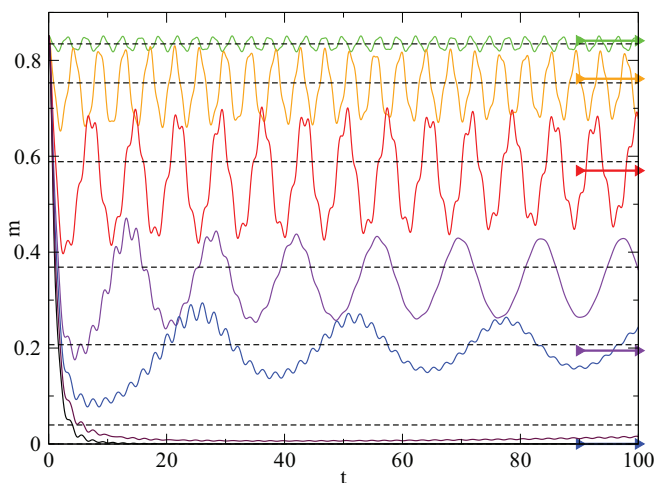


FIG. 2. (Color online) Time evolution of the staggered magnetization m for quenches $U_i = 4.0 \rightarrow U_f = 3.8, 3.2, 2.6, 2.2, 2.0, 1.8, 1.6$. The bold arrows indicate the corresponding thermal values m_{th} , while the black dashed lines indicate the long-time averages.

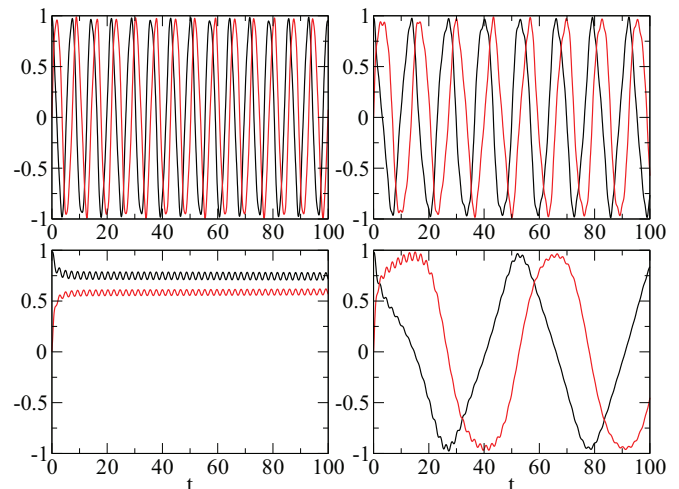


FIG. 3. (Color online) Time evolution of $\text{Re}(R_{A\uparrow})$ (black) and $\text{Im}(R_{A\uparrow})$ (red) for quenches $U_i = 4.0 \rightarrow U_f = 3.2, 2.6, 2.0, 1.6$ (clockwise order from top left).

Finally, from Fig. 6 we see that the long-time average of $|R_\sigma|^2$ increases in the limit of $U_f \rightarrow 0$, indicating that the AFM insulator actually melts into a PM metal.

B. $U_f > U_i$ quench

For quenches at $U_f < U_i$, the Gutzwiller dynamics is not different from the one obtained through single-particle methods such as the Hartree-Fock approximation; the magnetization shows an oscillatory behavior that turns eventually into a fast decay due to dephasing. Differences instead arise when $U_f > U_i$. Here, time-dependent Hartree-Fock predicts incorrectly that the magnetic order parameter never vanishes, whatever U_f is. This drawback is directly related to the inadequacy of Hartree-Fock in reproducing a decaying Néel temperature at large values of U , a feature that is instead captured by the Gutzwiller approach (see Fig. 1). In the assumption that the unitary evolution following the quantum quench brings the system in some thermal configuration at finite temperature, the higher the greater $|U_f - U_i|$, we can not only rationalize why time-dependent Hartree-Fock fails, but also anticipate, within the time-dependent Gutzwiller technique, a dynamical transition from an antiferromagnetic to a paramagnetic phase. Indeed, in the limit of very large $U_f > U_i$, when the frequency $\omega_1 \sim U_f$ gets much higher than the excitation energies of the Slater determinant, each $(\mathbf{k}, \mathbf{k} + \mathbf{Q})$ pseudospin evolves under an effectively slow magnetic field, hence the staggered magnetization averages again to zero due to dephasing.

We find confirmation of this expectation in the time evolution of $m(t)$ (see Fig. 4) and the main drive frequencies shown Fig. 5. In the limit of large U_f , a two-frequency oscillation pattern appears again, with a high frequency ω_1 that grows as $\propto U_f$ and a lower frequency associated with a vanishing mode which decays as $\propto |U_f - U_c^{U_f > U_i}|$ with the critical value of $U_c^{U_f > U_i} \approx 21.0$. We note that also in this regime the long-time average of the magnetization differs from the corresponding thermal value. Indeed, in Fig. 4 we see that for $U_f = 12.0$ the effective temperature has already

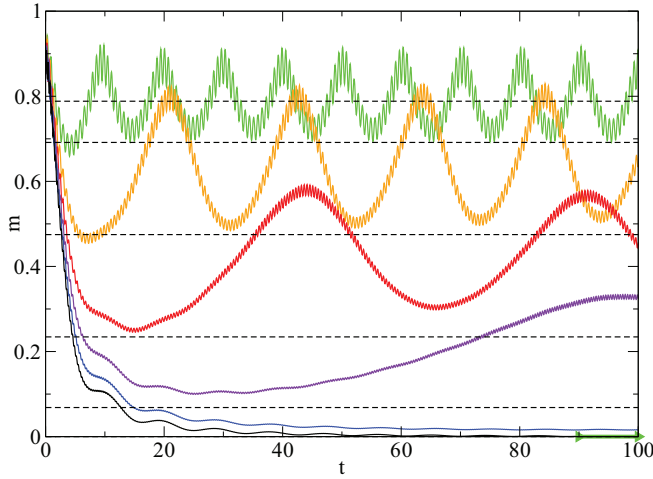


FIG. 4. (Color online) Time evolution of the staggered magnetization m for quenches $U_i = 4.0 \rightarrow U_f = 12.0, 14.0, 16.0, 18.0, 20.0, 22.0$. The green arrow indicates the thermal values m_{th} for $U_f = 12.0$ and shows that the effective temperature has already crossed the Néel temperature. The black dashed lines indicate the values of the long-time average.

crossed the Néel temperature, while the long-time average of the magnetization stays greater than zero, indicating the persistence of a nonequilibrium ordered state in accordance with the results of Ref. 7.

For smaller values of U_f , instead a less clear scenario appears. Indeed, in the range of values $5.8 \lesssim U_f \lesssim 8.4$ (vertical dashed lines of Fig. 5), although the main frequencies ω_1 and ω_2 can be still recognized by continuity from the large- and small- U_f limits, the Fourier power spectrum loses regularity and shows an increased number of broad peaks. In this interval of U_f , the long-time average of the magnetization increases while the renormalization factors diminish (see Fig. 6), suggestive of the systems driven towards a Mott-localized regime.

We note that Eqs. (15) and (17) admit a stationary solution identified by $R_\sigma = 0$ and energy equal to zero, which describes a trivial Mott-insulating state. We find that when the conserved energy after the quench is vanishing, which happens at $U_c^{\text{dyn}} \approx 8.2$ when $U_i = 4.0$, Eqs. (15) and (17) flow towards the above stationary solution (see Fig. 6), similar to what is found in the absence of magnetism in Ref. 9. We can shed some

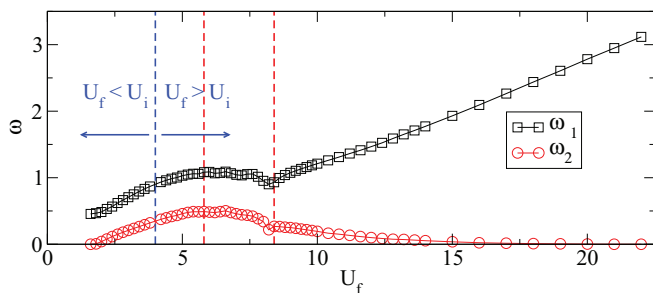


FIG. 5. (Color online) Behavior of the main drive frequencies ω_1 and ω_2 as a function of U_f . The two dashed red lines indicate the crossover region in which the Fourier power spectrum presents broad peaks.

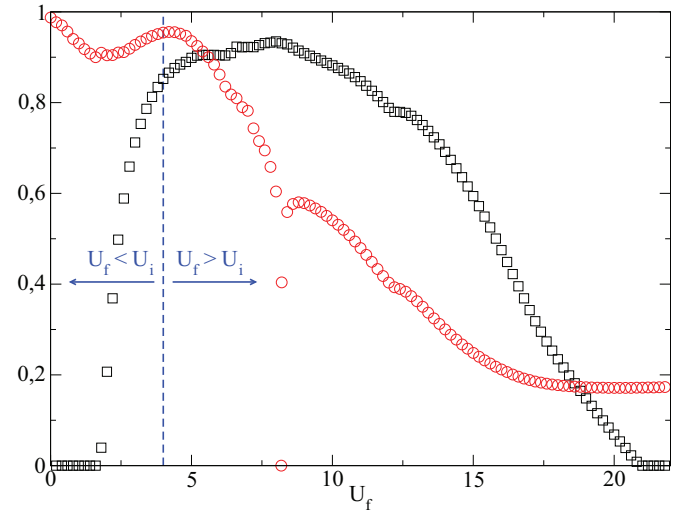


FIG. 6. (Color online) Long-time averages of the magnetization (black squares) and of $|R_\sigma|^2$ (red circles) as a function of U_f . At $U_f^c \approx 8.2$, the renormalization factor time average decays to zero, signaling the presence of the dynamical critical point.

light on this dynamical behavior by writing the Gutzwiller parameters as

$$\Phi_0 = \Phi_{\uparrow\downarrow} = \rho_0 e^{i\varphi_0}, \quad (21)$$

$$\Phi_\sigma = \rho_\sigma e^{i\varphi_\sigma}, \quad (22)$$

with $\rho_{0(\sigma)} \geq 0$ that, because of normalization, satisfy $2\rho_0^2 + \rho_\uparrow^2 + \rho_\downarrow^2 = 1$ and analyzing the quantity

$$\text{Re}\left(\frac{\Phi_\uparrow\Phi_\downarrow}{\Phi_0^2}\right) = \frac{\rho_\uparrow\rho_\downarrow}{\rho_0^2} \cos(2\varphi_0 - \varphi_\uparrow - \varphi_\downarrow) \equiv \frac{\rho_\uparrow\rho_\downarrow}{\rho_0^2} \cos\varphi. \quad (23)$$

Neglecting magnetism, which is the same as starting from $U_i = 0$, it was shown in Ref. 9 that the Mott-localized phase can be identified by the dynamics of the angle φ , which reproduces that of a classical pendulum. Below U_c^{dyn} , φ undergoes small oscillations around zero, hence Eq. (23) is positive. On the contrary, above U_c^{dyn} , $\cos\varphi$ starts precessing around the whole unit circle, and, in particular, is negative right in the regions where the double-occupancy probability $|\Phi_{\uparrow\downarrow}|^2 = \rho_0^2$ is lower. It follows that, for $U_f > U_c^{\text{dyn}}$, the quantity in Eq. (23) is on average negative. Exactly at U_c^{dyn} , ρ_0 vanishes exponentially, so that the long-time average of $\text{Re}\left(\frac{\Phi_\uparrow\Phi_\downarrow}{\Phi_0^2}\right)$ diverges and changes sign right at U_c^{dyn} (see Fig. 7 left panel). In the right panel of the same figure, we show that the same singular behavior persists also when the system is quenched from an AFM state. Even though in this case the angle φ is not bounded between $[0 : 2\pi]$ below U_c^{dyn} , due to the dynamics of the AFM order parameter, yet the time average has a well-defined sign that changes crossing a singularity at U_c^{dyn} .

This is suggestive of a dynamical Mott localization at $U_c^{\text{dyn}} \approx 8.2$, which has no equilibrium counterpart and separates two different antiferromagnetic insulators. We can not exclude that this transition may be an artifact of the Gutzwiller

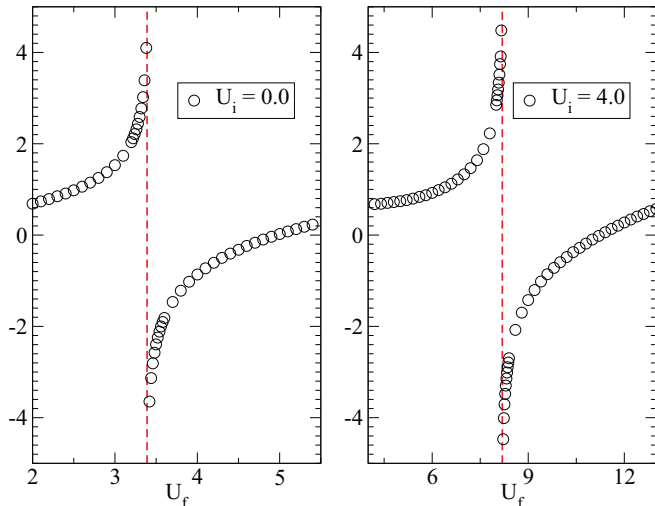


FIG. 7. (Color online) Long-time average of $\mathcal{O} = \text{Re}(\frac{\Phi_+ \Phi_-}{\Phi_0^2})$ in logarithmic units, i.e., $\text{sgn} \mathcal{O} \ln(|\mathcal{O}|)$, for different values of U_f . Both in the PM case (left panel) and in the AFM one (right panel), the dynamical critical point is evidenced by a sharp singularity.

technique, although we are tempted to give it a physical meaning. In order to clarify this point, we first introduce a more general definition of the quasiparticle residue $Z_{\mathbf{k}\sigma}$ through

$$Z_{\mathbf{k}\sigma} = |\langle \mathbf{k}\sigma, N+1 | c_{\mathbf{k}\sigma}^\dagger | 0, N \rangle|^2, \quad (24)$$

where $|0, N\rangle$ is the ground state with N electrons, assumed to have zero momentum and spin, and $|\mathbf{k}\sigma, N+1\rangle$ the lowest-energy state with $N+1$ electrons, momentum \mathbf{k} , and spin σ . $Z_{\mathbf{k}\sigma}$ defined by Eq. (24) coincides with the jump of the momentum distribution at the Fermi surface $|\mathbf{k}| = k_F$ for a Landau-Fermi liquid, but remains well defined also for an insulator, where it can be used to establish whether well-defined quasiparticles exist above the gap. Indeed, one can readily realize that $Z_{\mathbf{k}\sigma} = 1$ for a noninteracting band insulator. Therefore, one can in principle distinguish two different insulators: a ‘‘coherent’’ insulator akin to a band insulator with $0 < Z_{\mathbf{k}\sigma} \leq 1$, and an ‘‘incoherent’’ insulator, similar to an idealized Mott insulator, with $Z_{\mathbf{k}\sigma} = 0$ and no well-defined quasiparticles above the gap.

We then observe that, at zero temperature, $|R_\sigma|^2$ defined by Eq. (10) is just an estimate, within the Gutzwiller approximation, of $Z_{\mathbf{k}\sigma}$ above. Indeed, one can readily prove that

$$\begin{aligned} \langle \mathbf{k}\sigma, N+1 | c_{\mathbf{k}\sigma}^\dagger | 0, N \rangle &\stackrel{GW}{=} \langle \psi_N | c_{\mathbf{k}\sigma} \mathcal{P} c_{\mathbf{k}\sigma}^\dagger \mathcal{P} | \psi_N \rangle \\ &= R_\sigma. \end{aligned} \quad (25)$$

Here, we used the fact that the Gutzwiller wave function $\mathcal{P} |\psi_N\rangle$ [with $|\psi_N\rangle$ the N -particle Slater determinant that defines the variational wave function in Eq. (3)] is the variational estimate of $|0, N\rangle$ and that, within corrections $O(N^{-1})$, the best variational estimate of the $(N+1)$ -electron lowest-energy wave function with momentum \mathbf{k} and spin σ is just $|\mathbf{k}\sigma, N+1\rangle \simeq \mathcal{P} c_{\mathbf{k}\sigma}^\dagger |\psi_N\rangle$, with the same \mathcal{P} as for N electrons. Equation (25) remains valid also in the time-dependent case where the evolution of the ground state, being a pure state, is approximated by Eq. (3).

We then arrive to the conclusion that our dynamical transition separates two different antiferromagnetic insulators in the above meaning, one characterized by a finite Z and the other by a vanishing one. It is worth mentioning that at equilibrium and zero temperature, all evidences indicate that Z of Eq. (24) is everywhere finite in the antiferromagnetic insulating phase of the Hubbard model at any value of U , as confirmed by DMFT (Ref. 18) and by quantum Monte Carlo simulations on the t - J model.¹⁹ In other words, even at very large U where the Mott’s physics dominates and local moments are already well formed, the antiferromagnet has coherent quasiparticles above the gap. We actually believe that, as soon as long-range magnetic order sets in below the Néel temperature, the quasiparticle residue Z becomes finite at equilibrium. In fact, the onset of long-range order is accompanied at large U by a hopping energy gain, through the spin exchange t^2/U , hence by a raise of lattice coherence that we think has to be associated with an increase of Z . That is why we think that the dynamical transition that we observe has no equilibrium counterpart in the whole U versus temperature phase diagram.

We conclude mentioning that the main results presented above at fixed $U_i = 4$ remain qualitatively the same also at different U_i . We indeed verified the presence of the critical points at which the magnetization vanishes $U_c^{U_f \leq U_i}$ and the presence of the dynamical critical point $U_i < U_c^{\text{dyn}} < U_c^{U_f > U_i}$ for all values of $U_i < 10.0$.

IV. CONCLUDING REMARKS

We have shown that the time-dependent Gutzwiller technique, in spite of its simplicity, is able to reproduce the main features of a quench dynamics from an antiferromagnetic state found by time-dependent DMFT, such as the existence of nonthermal magnetically ordered states that disappear above dynamical critical points, both suddenly decreasing or increasing the value of the Hubbard U . In addition, we have found evidence of an additional dynamical transition that occurs at large U , which we interpret as a dynamical Mott transition separating two different antiferromagnetic nonequilibrium states, one characterized by a finite quasiparticle residue and the other by a vanishing one. Since the quasiparticle residue Z in an antiferromagnet can not be extracted by any static property (unlike in a paramagnet where, at zero temperature, Z is the jump of the momentum distribution at the Fermi surface), but requires calculating for instance the full out-of-equilibrium self-energy, its dynamical behavior was not addressed by DMFT in Refs. 7 and 8. Although we can not exclude that the vanishing of Z that we observe could be an artifact of the Gutzwiller technique, nevertheless this result is intriguing, as it entails the existence in out of equilibrium of an incoherent antiferromagnet, hence worth to be further investigated.

ACKNOWLEDGMENTS

We thank A. Amaricci for very helpful suggestions. This work has been supported by the European Union, Seventh Framework Programme, under the project GO FAST, Grant Agreement No. 280555.

- ¹I. Bloch, J. Dalibard, and W. Zwerger, *Rev. Mod. Phys.* **80**, 885 (2008).
- ²A. L. Cavalieri, N. Muller, T. Uphues, V. S. Yakovlev, A. Baltuska, B. Horvath Schmidt, L. Blumel, R. Holzwarth, S. Hendel, M. Drescher *et al.*, *Nature (London)* **449**, 1029 (2007).
- ³L. Perfetti, P. A. Loukakos, M. Lisowski, U. Bovensiepen, H. Berger, S. Biermann, P. S. Cornaglia, A. Georges, and M. Wolf, *Phys. Rev. Lett.* **97**, 067402 (2006).
- ⁴P. Beaud, S. L. Johnson, E. Vorobeva, U. Staub, R. A. De Souza, C. J. Milne, Q. X. Jia, and G. Ingold, *Phys. Rev. Lett.* **103**, 155702 (2009).
- ⁵D. Fausti, R. I. Tobey, N. Dean, S. Kaiser, A. Dienst, M. C. Hoffmann, S. Pyon, T. Takayama, H. Takagi, and A. Cavalleri, *Science* **331**, 189 (2011).
- ⁶G. Mazza and M. Fabrizio, *Phys. Rev. B* **86**, 184303 (2012).
- ⁷P. Werner, N. Tsuji, and M. Eckstein, *Phys. Rev. B* **86**, 205101 (2012).
- ⁸N. Tsuji, M. Eckstein, and P. Werner, *Phys. Rev. Lett.* **110**, 136404 (2013).
- ⁹M. Schiró and M. Fabrizio, *Phys. Rev. Lett.* **105**, 076401 (2010).
- ¹⁰M. Schiró and M. Fabrizio, *Phys. Rev. B* **83**, 165105 (2011).
- ¹¹M. Sandri, M. Schiró, and M. Fabrizio, *Phys. Rev. B* **86**, 075122 (2012).
- ¹²M. Fabrizio, in *New Materials for Thermoelectric Applications: Theory and Experiment*, NATO Science for Peace and Security Series B: Physics and Biophysics, edited by V. Zlatić and A. Hewson (Springer, Berlin, 2013), pp. 247–272.
- ¹³M. Sandri, M. Capone, and M. Fabrizio, *Phys. Rev. B* **87**, 205108 (2013).
- ¹⁴S. A. Hamerla and G. S. Uhrig, *Phys. Rev. B* **87**, 064304 (2013).
- ¹⁵S. A. Hamerla and G. S. Uhrig, arXiv:1307.3438.
- ¹⁶N. Lanatà, P. Barone, and M. Fabrizio, *Phys. Rev. B* **78**, 155127 (2008).
- ¹⁷N. Lanatà, Y.-X. Yao, C.-Z. Wang, K.-M. Ho, J. Schmalian, K. Haule, and G. Kotliar, arXiv:1305.3950.
- ¹⁸R. Chitra and G. Kotliar, *Phys. Rev. Lett.* **83**, 2386 (1999).
- ¹⁹M. Brunner, F. F. Assaad, and A. Muramatsu, *Phys. Rev. B* **62**, 15480 (2000).